NRC Research Press

ARTICLE

Constant pH simulations with the coarse-grained MARTINI model — Application to oleic acid aggregates

W.F. Drew Bennett, Alexander W. Chen, Serena Donnini, Gerrit Groenhof, and D. Peter Tieleman

Abstract: Long chain fatty acids are biologically important molecules with complex and pH sensitive aggregation behavior. The carboxylic head group of oleic acid is ionizable, with the pK_a shifting to larger values, even above a value of 7, in certain aggregate states. While experiments have determined the macroscopic phase behavior, we have yet to understand the molecular level details for this complex behavior. This level of detail is likely required to fully appreciate the role of fatty acids in biology and for nanoscale biotechnological and industrial applications. Here, we introduce the use of constant pH molecular dynamics (MD) simulations with the coarse-grained MARTINI model and apply the method to oleic acid aggregates and a model lipid bilayer. By running simulations at different constant pH values, we determined titration curves and the resulting pK_a for oleic acid in different environments. The coarse-grained model predicts positive pK_a shifts, with a shift from 4.8 in water to 6.5 in a small micelle, and 6.6 in a dioleoylphosphatidylcholine (DOPC) bilayer, similar to experimental estimates. The size of the micelles increased as the pH increased, and correlated with the fraction of deprotonated oleic acid. We show this combination of constant pH MD and the coarse-grained MARTINI model can be used to model pH-dependent surfactant phase behavior. This suggests a large number of potential new applications of large-scale MARTINI simulations in other biological systems with ionizable molecules.

Key words: constant pH molecular dynamics, fatty acids, oleic acid, MARTINI model, coarse-grained model.

Résumé : Les acides gras à longue chaine sont des molécules importantes sur le plan biologique, dont le comportement d'agrégation est complexe et sensible au pH. Le groupe carboxyle de tête de l'acide oléique est ionisable, le pKa évoluant vers des valeurs plus élevées, même supérieures à 7, dans certains états agrégés. Si des expériences ont permis de déterminer le comportement dans la phase macroscopique, on n'a pas encore élucidé les détails de niveau moléculaire de ce comportement complexe. Ce niveau de détail est vraisemblablement nécessaire pour apprécier pleinement le rôle des acides gras en biologie, ainsi que pour les applications biothechnologiques et industrielles nanoscopiques. Ici, nous présentons l'utilisation de simulations de dynamique moléculaire à pH constant à l'aide du modèle gros-grain MARTINI et nous appliquons la méthode aux agrégats d'acide oléique et à un modèle de bicouche lipidique. En exécutant les simulations à différents pH, nous déterminons les courbes de titrage et le pKa résultant de l'acide oléique dans diverses conditions. Le modèle gros-grain prédit des changements positifs de pKa, lequel passe de 4,8 dans l'eau à 6,5 dans une petite micelle, et à 6,6 dans une bicouche de DOPC, qui sont similaires aux estimations expérimentales. La taille des micelles s'accroît quand le pH augmente et corrèle avec la fraction d'acide oléique déprotoné. Nous montrons que l'on peut se servir de cette combinaison de dynamique moléculaire à pH constant et du modèle de simulation gros-grain MARTINI pour modéliser le comportement variant avec le pH dans la phase tensioactive. Cela suggère un grand nombre de nouvelles applications possibles de simulations MARTINI à grande échelle pour d'autres systèmes biologiques comprenant des molécules ionisables. [Traduit par la Rédaction]

Mots-clés : dynamique moléculaire à pH constant, acides gras, acide oléique, modèle Martini, modèle gros-grain.

Introduction

Surfactants are crucial chemicals in our daily lives, from soaps and detergents to food processing and biotechnology. Fatty acid aggregation is important for a wide range of applications. Fatty acids form vesicles that are capable of self-replication,[1] are involved in creating and maintaining a pH gradient during growth,[2] and are involved in the disruption of the mitochondrial proton gradient during nonshivering thermogenesis.[3] Fatty acids combined with relatively large cationic penetrating amphiphiles are able to dissipate the pH gradient across a vesicle.[4] Lauric acid was recently used to coat the surface of iron nanoparticles for improved dispersibility.[5] Lauric acid and other short and medium chain fatty acids have been shown to have antimicrobial activity.[6] Given their simple chemical structure, fatty acids provide a valuable model system for simulations and experiments, with a large number of possible applications. In particular, they can be thought of as a model system for physiologically important ionizable lipids such as phosphatidylserine and phosphatidic acid lipids.

Oleic acid (OA) is a long chain fatty acid with an 18-carbon tail with one double bond and a carboxylic head group. The phase behavior of oleic acid has been studied extensively.[7,8] At low pH (<7), OA is mostly protonated and an oil phase is observed; at intermediate pHs (7–9), bilayers and vesicles are observed; at high

Received 6 January 2013. Accepted 3 April 2013.

W.F.D. Bennett, A.W. Chen, and D.P. Tieleman. Department of Biological Sciences and Institute for Biocomplexity and Informatics, University of Calgary, 2500 University Dr. NW, Calgary, AB T2N 1N4, Canada.
S. Donnini. Department of Theoretical and Computational Biophysics, Max Planck Institute for Biophysical Chemistry, Am Fassberg 11, 37077 Göttingen, Germany.
G. Groenhof. Department of Chemistry and Nanoscience Center, University of Jyväskylä, P.O. Box 35, FI-40014 Jyväskylä, Finland.
Corresponding author: D. Peter Tieleman (e-mail: tieleman@ucalgary.ca).

This article is part of a Special Issue dedicated to Professor Dennis Salahub in recognition of his contributions to theoretical and computational chemistry.

pHs (>9), OA is mostly ionized, and micelles and other structures are observed.[7] The pK_a of oleic acid as a monomer in bulk water is difficult to measure due to its low solubility and tendency to aggregate. The pK_a values of several shorter chain fatty acids are near 4.8.[9]

There have been a number of molecular dynamics (MD) simulations studying oleic acid and other long chain fatty acids.[10–14] Oleic acid has been simulated in a dipalmitoylphosphatidylcholine (DPPC) bilayer using coarse-grained MD simulations.[10] Partial phase diagrams for mixtures of sodium laurate and oleate were studied using atomistic simulations, reproducing the experimentally observed micellar, hexagonal, and lamellar phases.[12] A single lauric acid was recently simulated in ionic and nonionic micelles using atomistic constant pH MD simulations.[15] A subsequent study investigated the aggregation of 20-mers of lauric acid using constant pH simulations.[16] In both micelle environments, lauric acid exhibited positive pK_a shifts compared to in water.

Modeling the effect of pH on aggregation is challenging because on the one hand the timescale precludes the use of quantum chemical approaches, while on the other hand the chemical nature of proton transfer precludes the use of classical molecular dynamics. To overcome this problem, approaches have been developed that allow the protonation state of ionizable groups to change dynamically during molecular dynamics simulations.[17–21] These changes are driven by interactions with the local environment and pH of the solution, which is now a parameter in the simulation.

Coarse-grained (CG) molecular dynamics simulations have been used extensively to model surfactant systems.[22–26] CG systems allow much larger systems to be simulated for longer timescales. For long timescale processes such as vesicle fusion, aggregation, and lipid domain formation that are beyond the capacity of current atomistic simulations, CG models can be used. In MARTINI, on average four nonhydrogen atoms are combined into a single interaction site, while attempting to maintain a reasonable degree of chemical specificity. Here, we use MARTINI to model OA surfactants and dioleoylphosphatidylcholine (DOPC) lipids. To the best of our knowledge, this is the first time that constant pH MD has been used with a coarse-grained model. OA was chosen as it has a simple chemical structure, has complex pH-dependent phase behavior, and is important in a wide range of applications. Due to computational constraints, we simulated small aggregates of OA, a 20-mer and a 30-mer, and therefore cannot directly compare our results with experimental phase behavior. We also simulated OA in a DOPC bilayer using constant pH MD simulations.

Methods

CG simulations

We ran simulations of oleic acid aggregates using the standard MARTINI model[27] and the MARTINI polarizable water model.[28] In the original MARTINI model, four waters were modeled with a single Lennard-Jones particle. Polarizable MARTINI water also represents four waters, but with three particles, a positive and negative partial charge bonded to a central Lennard-Jones particle.[28] Oleic acid is modeled with five hydrophobic beads, and a single hydrophilic bead for the head group. The head group bead is negatively charged for oleate and neutral for oleic acid, and they have different Lennard-Jones interactions. These parameters were adapted from aspartate and aspartic acid from the MARTINI 2.1 amino acid force field.[27]

Standard MARTINI molecular dynamics run parameters were used for the simulations,[27] with the additional parameters for constant pH simulations discussed below. We used a 20 fs time step, updating the neighbor list every 10 steps. For the Lennard-Jones interactions, a switch potential was employed from 0.9 to 1.2 nm. Electrostatic interactions were determined with Coulomb's equation with a 1.2 nm cutoff and a shifted potential from 0 to 1.2 nm. A dielectric constant of 2.5 was used for screening of charged interactions consistent with the MARTINI parameterization. Simulations were run at 330 K using the Berendsen weak-coupling method and a coupling constant of 1 ps.[29] For the micelle systems, isotropic pressure coupling, with a pressure of 1 bar (1 bar = 100 kPa) and a 1 ps coupling constant, was used with the Berendsen weak-coupling method.[29] We used semi-isotropic coupling for the DOPC bilayer system with pressures of 1 bar and 1 ps coupling constants, both lateral and normal to the plane of the bilayer.

Constant pH methodology

We used a recent implementation of constant pH molecular dynamics,[20] which is based on a modified version of GROMACS 3.3.3.[30,31] This method allows ionizable residues to change protonation state during the course of a simulation. Here, we first give a brief general overview of the method and then provide the details about the constant pH simulation setup used in this work. For a more detailed presentation of the method, we refer the reader to a previous implementation paper.[20]

As in more common free energy calculations, different protonation states of a titrating group are coupled via a λ parameter, in such a way that the residue is protonated at λ = 0 and deprotonated at λ = 1. The energy function of the system is a linear combination of the potential energy of the protonated and deprotonated state and some additional λ-dependent energy functions that will be specified later:

$$V(\lambda) = (1-\lambda)V^{\mathrm{prot}} + \lambda V^{\mathrm{deprot}} + U(\lambda) + \lambda \ln 10\left(\mathrm{p}K_a^{\mathrm{ref}} - \mathrm{pH}\right) - \Delta\tilde{G}_{\mathrm{ref}}^{\mathrm{FF}}(\lambda) \quad (1)$$

where V^{prot} (V^{deprot}) is the total potential energy function of the system if the group is protonated (deprotonated). The reference pK_a^{ref} is the experimental reference pK_a value of an OA in water (4.8).[9] $\Delta\tilde{G}_{\mathrm{ref}}^{\mathrm{FF}}(\lambda)$ and $U(\lambda)$ are a correction term and a barrier potential that are described below.

In contrast to the established thermodynamic integration approach, λ is treated as a free, dynamic coordinate with mass, m_λ, very much like the Cartesian coordinates of all atoms. Accordingly, λ is subject to a force

$$F_\lambda = -\frac{\partial V(\lambda)}{\partial \lambda}$$

To constrain the λ interval, we introduce a dynamic angular coordinate, θ, and λ is redefined as the projection

$$\lambda = r\cos(\theta) + \frac{1}{2}$$

For r, we take $r = \frac{1}{2} + \sigma$ with an appropriate fluctuation size, σ. We use a value of $\sigma = 0.05$, because with this value the average λ at the physical states was ~0 (protonated state) and ~1 (deprotonated state).[20] The actual dynamics takes place in θ space, and is subject to a force

$$F_\theta = -\frac{\partial V(\lambda(\theta))}{\partial \theta} = r\sin(\theta)\frac{\partial V(\lambda(\theta))}{\partial \lambda}$$

The biasing potential, $U(\lambda)$, is a function of λ that acts as a barrier between λ 0.1 and λ 0.9. In this way, it controls the frequency of the transition between the protonation states and that limits the time spent at the unphysical intermediate states:

The biasing potential is constructed by interpolating cubic splines between seven points between λ 0.1 and 0.9: (0.1, 0), (0.2,

h/2.25), (0.3, h/1.25), (0.5, h), (0.7, h/1.25), (0.8, h/2.25), and (0.9, 0) with h being the height of the barrier. We used a value of 10 kJ/mol for h.

To model protonation events at a given pH we included the effect of the solution's pH (second term in eq. (1)) and contributions to the free energy of protonation due to breaking and forming chemical bonds, which are not described by the MARTINI force field, in the potential energy function (last term in eq. (1)). The latter term, $\Delta\tilde{G}^{FF}_{ref}(\lambda)$, shifts the protonation equilibrium in the potential energy function, $V(\lambda)$, such that for a simulation under the reference conditions (a single OA in water), the free energy difference between the end states is only dependent on the external pH. When embedded in a different environment, such as a bilayer or micelle, the long-range interactions with that environment (first two terms in eq. (1)) can shift that equilibrium and therefore alter the OA's pK_a value. To determine $\Delta\tilde{G}^{FF}_{ref}(\lambda)$ we first computed the free energy of deprotonating a single OA in water by means of the thermodynamic integration technique[32] and fitted a third order polynomial function to the derivative of the free energy with respect to l:

$$\frac{dG}{dl} = \left\langle \frac{\partial V^{CG}(l)}{\partial l} \right\rangle_l$$

Here, V^{CG} is the standard MARTINI coarse-grained force field potential energy function, linearly interpolated along the coupling parameter, l, between protonated and nonprotonated OA, which should not be confused with the energy function for the λ dynamics in eq. (1).

The reference deprotonation free energies were obtained as follows: A single OA was placed in a cubic box filled with 1020 water beads. The reference free energy simulations consisted of 11 separate 100 ns MD, with the coupling parameter, l, increased from 0 to 1 with a 0.1 spacing, thus deprotonating the OA. Figure 1 shows the profile obtained for the change of protonated oleic acid (OA^{OH}) in water to negatively charged deprotonated oleate (OA^{1-}). The size and shape of the box in the reference and the monomer constant pH simulations were identical.

In the constant pH simulations, a stochastic Andersen thermostat was used to maintain the temperature of the λ subsystem at 320 K with a coupling time of 0.02 ps. This coupling time in combination with a mass, m_λ, of 20 amu and barrier height of 10 kJ/mol yields a small ratio between transition time and residence time.

Finally, we remark that during the simulation, the total charge is allowed to fluctuate. Although this can lead to artifacts if Ewald summation techniques were used, it is of no concern here because we using a shifted cutoff scheme for which the MARTINI force field has been parameterized.[27,28]

Systems

Figure 2 shows the systems we have simulated: OA as a monomer in bulk water, in micelles with 20 and 30 OA molecules, and in a DOPC bilayer. For the micelles, OAs were initially randomly dispersed in a box of water and aggregated into a stable micelle rapidly. We used a preformed DOPC bilayer and inserted a single OA. We ran the monomer constant pH simulations for 1 μs, 100 ns for the 20-mer, 50 ns for the 30-mer, and 100 ns for the DOPC bilayer. The constant-pH algorithm scales linearly with the number of titratable groups, limiting the total number of ionizable residues we are able to simulate in a single simulation.

Titration curves

To determine titration curves, we ran constant pH simulations at a range of pH values, with each fatty acid treated as ionizable. For each monomer, we determined the fraction of time spent deprotonated ($\lambda > 0.9$). Each monomer is then treated as an independent sample, from which we determined the mean and standard error of the mean for the fraction of deprotonated OA at each pH. These were then fit with the Hill equation:

$$S(\text{deprot}) = \frac{1}{10^{n(pK_a - pH)} + 1}$$

Here, S is the fraction of charged OA. From the fits we obtain estimates for the bulk pK_a of OA in different aggregation states. The Hill coefficient, n, gives the degree of cooperativity ($n > 1$) or anticooperativity ($n < 1$). When n is equal to 1, Henderson–Hasselbalch behavior is observed.

Fig. 1. Monomer free energy calculation. (A) Schematic showing the CG model of OA^{OH} and OA^{1-}. (B) Results from a thermodynamic integration calculation of a single OA in a box of water. The fit is a third-order polynomial ($y = -1.0268x^3 - 19.673x^2 - 70.567x - 2.4709$). Please view the article online for the colour version.

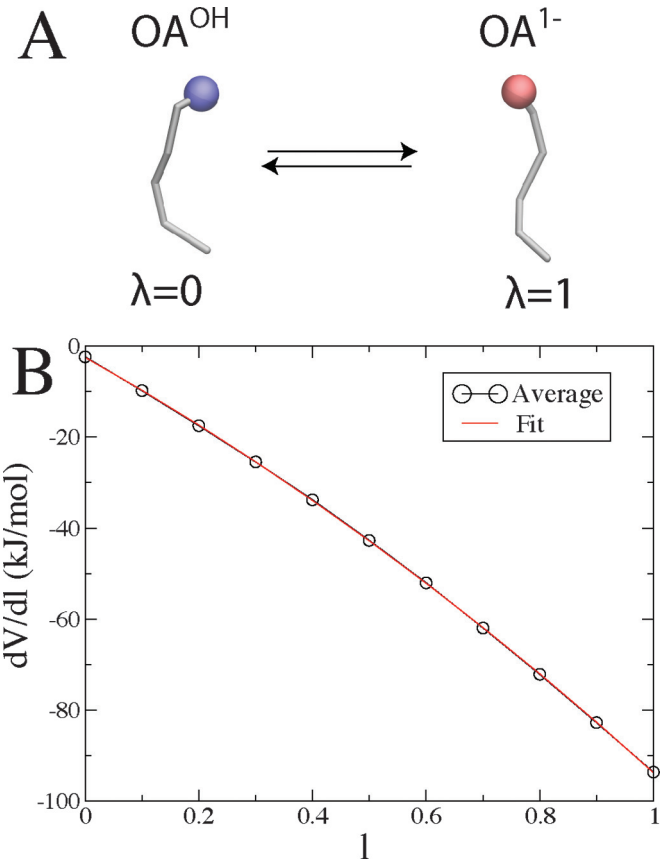

Results

Titration as a monomer

To first test whether the MARTINI model was suited for constant pH MD, we determined the titration curve for a single oleic acid in bulk water. We ran a series of constant pH simulations at different pH conditions, and determined the fraction of time the titratable groups are deprotonated. Figure 3A shows how the titration state changes between λ values of –0.05 and 1.05 during simulations at pH values below, near, and above the pK_a. At pH conditions well above or below the pK_a the OA stays close to either 0 or 1, but attempts to cross are observed. Near the pK_a there are many crossings between 0 and 1 or protonated and deprotonated, respectively. Figure 3B shows the titration curve we obtain with the MARTINI model of OA. We fit the curve to the Hill equation (red line), with a pK_a of 4.8 and a Hill coefficient of 0.91. This is the

Fig. 2. OA systems used in this work. Water is shown as orange sticks, OA in grey with a red sphere for the carboxylic head group, and DOPC in grey with grey spheres for the phosphate and choline beads. Please view the article online for the colour version.

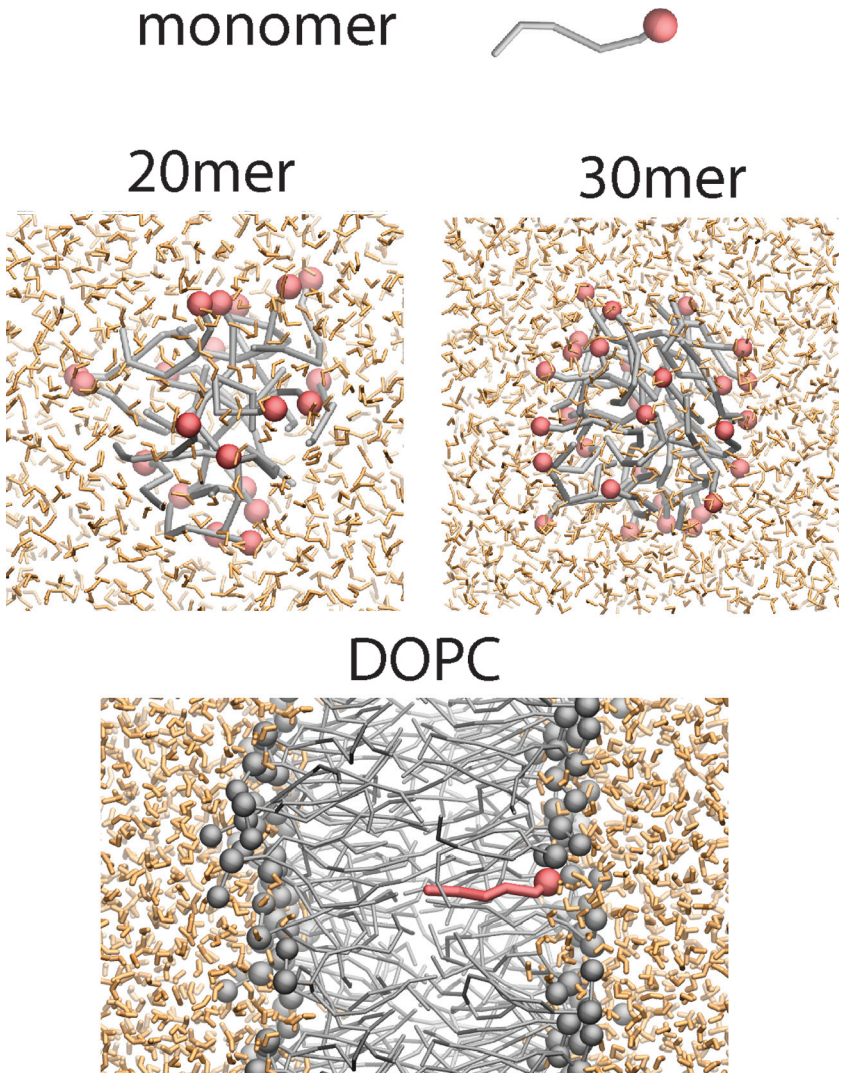

pK_a we used as the reference state of water, suggesting that constant pH MD and MARTINI model are technically compatible and can thus be combined.

Titration in micelles

We ran simulations of 20 and 30 OAs aggregated into micelles. Due to the low solubility of OA all the monomers were part of the preformed aggregate for all of the simulations and all pH conditions. The titration curves for the 20-mer and 30-mer are shown in Fig. 4. The curves are very similar for both the 20- and 30-mer micelles. Compared to the monomer, we observed substantially shifted titration curves, with a less steep slope, and larger pK_a values. From the fit to the Hill equation, we find that for a 20-mer the pK_a is 6.3 with a Hill coefficient of 0.51. For the 30-mer, we estimate OA to have a pK_a of 6.5 and a Hill coefficient of 0.49. As the aggregate becomes larger, the pK_a further increases.

Snapshots of the aggregates at the different pH values are shown in Fig. 5 with the protonation state of each monomer represented by its color. These are static snapshots, but the dynamic nature of these systems must be stressed.

Figure 6 shows the radius of gyration for the micelles as a function of the pH. We find a curve similar in shape to the titration curves, shown in Fig. 6C for comparison. At lower pH values the OA^{OH} predominates, and the micelle has a lower radius of gyration, while at higher pH values the OA^{1-} forms the majority, and the micelle has a larger radius of gyration.

Titration in a DOPC bilayer

We simulated one oleic acid molecule in a DOPC bilayer using constant pH MD simulations. The fatty acid sits in the membrane with the head group near the glycerol backbone, and the long tail in the hydrophobic bilayer as seen in Fig. 2.

Figure 7 shows the titration curve for a single OA in a DOPC bilayer. From the fit, a Hill coefficient of 0.96 and a pK_a of 6.6 were determined for OA in a DOPC bilayer. Figure 8 shows the partial density profile for the DOPC bilayer, at low pH (2) when the head group is protonated and able to cross the bilayer, and at high pH (15) when it is charged and stays on one side of the bilayer for the entire 100 ns simulation. When the head group is deprotonated and charged, the density is further out from the bilayer center, to interact with the charged DOPC head groups.

Discussion

pK_a shifts

For the OA monomer, we found a titration curve that was close to the expected Henderson–Hasselbalch equation, with a Hill coefficient of 0.91. The titration curves for OA in different aggregate

Fig. 3. Monomer titration. (A) The fluctuation of OA's protonation state for the final 50 ns of the simulation. (B) Titration curve for OA and the fit with the Hill equation. Please view the article online for the colour version.

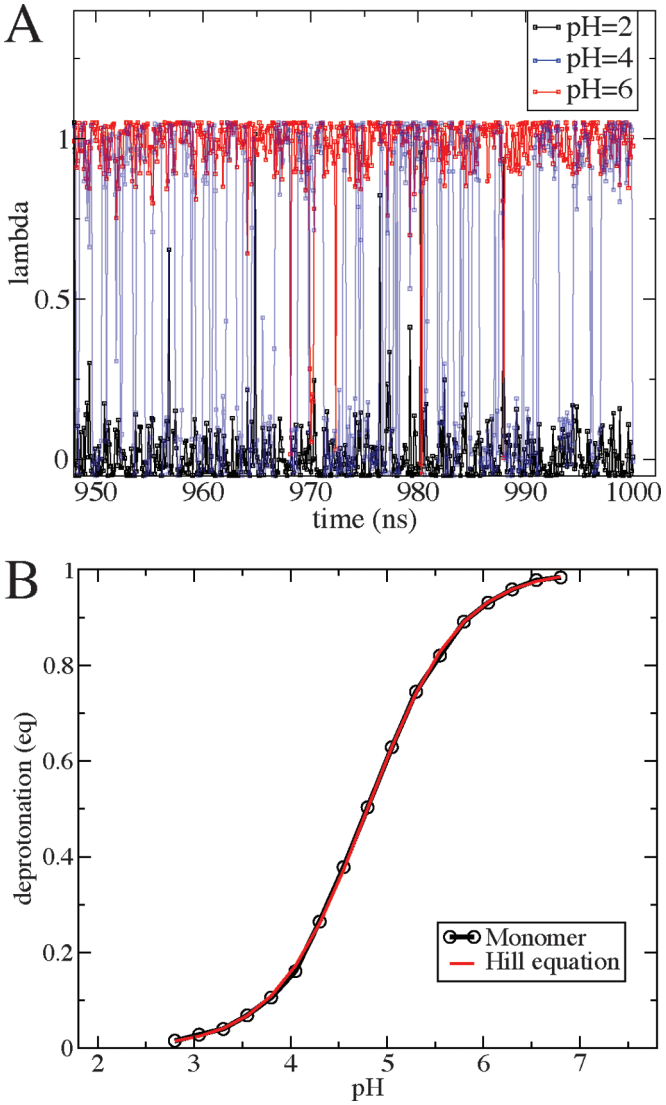

states were both shifted to larger values, and the curves were less steep. This large increase in pK_a means that as monomers in water at pH 7, there would be practically no protonated OA^{OH}. A considerable fraction of OA would be protonated in the micelles and in a DOPC bilayer at neutral pH conditions. This drastic shift in ionization state would have a large effect on the properties and physicochemical behavior of OA.

The positive shifts in pK_a match the expected trend from experimental phase diagrams of OA.[7] We cannot directly compare our current simulations of OA with experiment due to finite system sizes and our choice of 20- and 30-mers, which may in fact not be stable thermodynamic states. Future work on larger systems will be needed to directly compare to experimental results, where lamellar structures are observed for oleic acid.

The reasons for the positive shift in pK_a are likely complex, and will require future work to fully understand. Electrostatic repulsion between the OA^{1-}'s in the aggregates might be used to explain the pK_a shifts. In an aggregate, having one deprotonated and negatively charged OA will reduce the probability that neighboring OA's will also be deprotonated. Our results predicting a positive shift in pK_a match previous constant pH MD simulations using an atomistic model of lauric acid.[16]

Fig. 4. Titration curves for oleic acid aggregates. (A) Titration of a 20-mer aggregate of OA with the titration points of the the 20 individual OA monomers shown as points. The mean and standard error of the mean for all 20 OAs is shown, along with a fit to the Hill equation. The titration curve for a monomer in bulk water is shown for comparison. (B) The same as (A), but for a 30-mer aggregate. The points for all 30 OAs are brown squares. Please view the article online for the colour version.

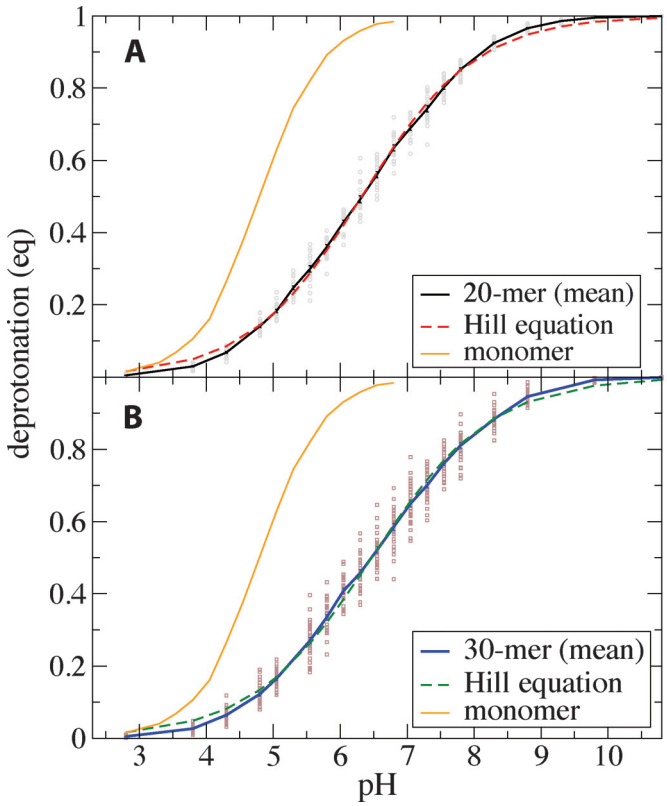

The amount of water interacting with the OA could also explain the shifts in pK_a. When there is more water to interact with, the titration behavior would be more similar to a monomer OA. In aggregates, the OA head group "experiences" a different and heterogeneous chemical environment, with less exposure to water, compared to a monomer in water. Taking this reasoning to the extreme, without any water the pK_a would shift to extremely high values, as having a desolvated negatively charged OA exposed to bulk hydrocarbon would be too energetically expensive. Indeed, we previously observed shifts in pK_a of aspartate and glutamate to ~16 at the center of a DOPC bilayer using atomistic simulations.[33]

Besides a positive shift in pK_a, for the micelles we also observed a large degree of anticooperativity in the titration curves, with Hill coefficients near 0.5. This behavior might again be explained using the electrostatic repulsion arguments mentioned previously. The multibody interactions between individuals in the aggregate could also explain this trend. As individual molecules change from protonated to deprotonated, the size of the aggregate changes, as illustrated by the similarity between the radius of gyration curves and the titration curves (Fig. 6). The protonated OA^{OH} prefers the larger mostly deprotonated aggregate, while the OA^{1-} prefers the smaller mostly protonated aggregate. This behavior would result in anticooperativity; both species have more favorable interactions with molecules of the opposite protonation state.

Fig. 5. Snapshots of the micelles during the constant pH simulations. The OA tails are grey lines, and the head groups of OAs are spheres, colored by their respective ionization state, with red OA^{1-} and blue OA^{OH}. Please view the article online for the colour version.

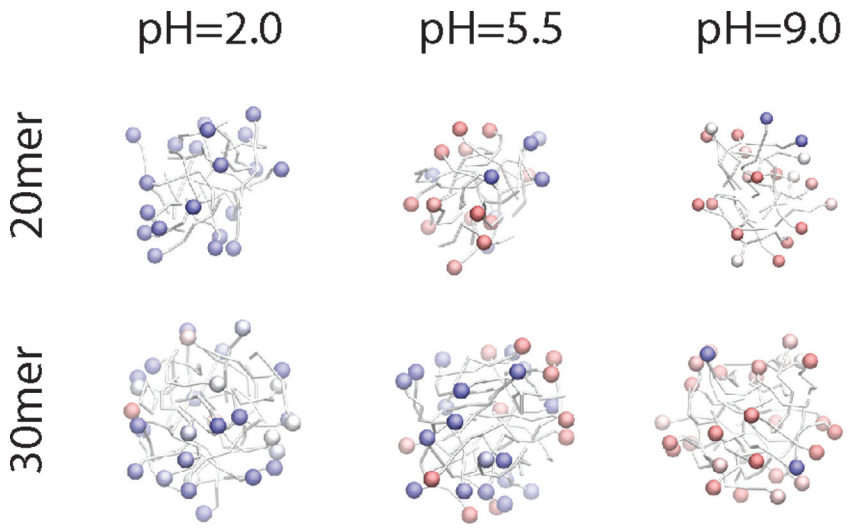

Fig. 6. (A) and (B) Radius of gyration for the micelles at different pH conditions. The radius of gyration was determined using the program g_gyrate from GROMACS. (C) Titration curves for the micelles for reference. Please view the article online for the colour version.

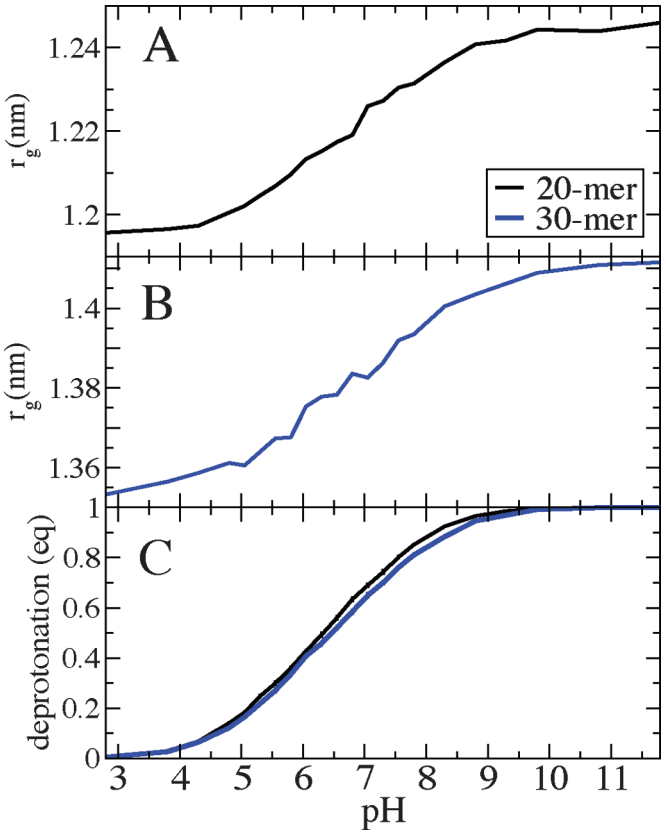

For OA in a DOPC bilayer, the MARTINI model predicts a pK_a of 6.6. This compares reasonably well to the value of 7.2–7.4 for stearic acid in an egg phosphatidylcholine (PC) bilayer[34] and 7.5 for oleic in an egg PC bilayer.[35] Electrostatic repulsion may also be used to explain the titration curve shifts in the micelles, in the bilayer, where the OA^{1-} head group is near the negatively charged phosphates of DOPC.

Fig. 7. OA titration curve in a DOPC bilayer. The curve is fitted to the Hill equation. The monomer titration curve in water is shown for reference. Please view the article online for the colour version.

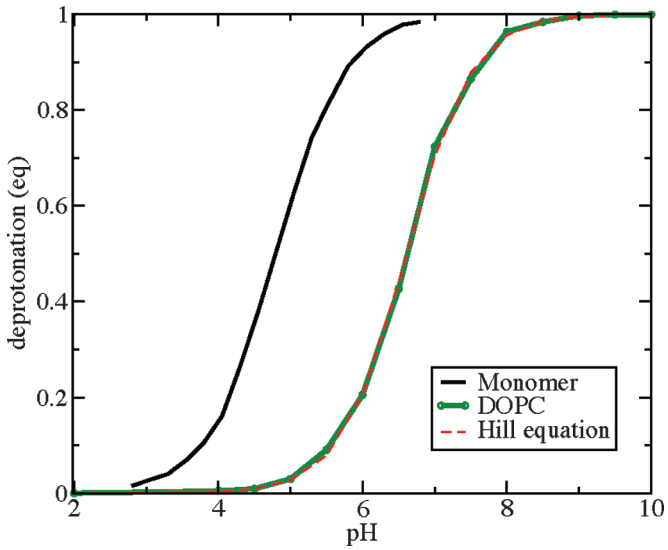

Model

By using the MARTINI model we can run longer timescale simulations of the constant pH approach, bringing biologically interesting questions within reach of simulations. The agreement between the CG model and experiment for the pK_a of OA in a PC bilayer is very good, but coarse-grained models have limitations in the accuracy and detail of their representation of the system of interest. In one example, we previously showed that the MARTINI model did not accurately reproduce the formation of pores in PC bilayers compared to atomistic results.[36] Understanding the limitations of a model is important for future use and refinement.

It will be important to study these aggregates using an atomistic model, and combining methods, where the aggregates from the CG simulations could be converted to atomistic representation, and vice versa. We previously determined the change in pK_a for the titratable amino acids from water through a DOPC bilayer, which could be used for parameterization.[33] Qualitatively our results of the positive shift in pK_a of long chain fatty acids in micelle states compare well to other recent atomistic simulations of lauric acid micelles with constant pH MD.[16] It will be

Fig. 8. (A) Snapshot of the DOPC bilayer system as colored in Fig. 1. (B) Partial density profile for the DOPC bilayer. (C) Density profile for the OA head group at pH 2 (magenta curve) and pH 15 (orange curve) in the DOPC bilayer. For clarity, the phosphate and choline densities were arbitrarily divided by 20 in (C). Please view the article online for the colour version.

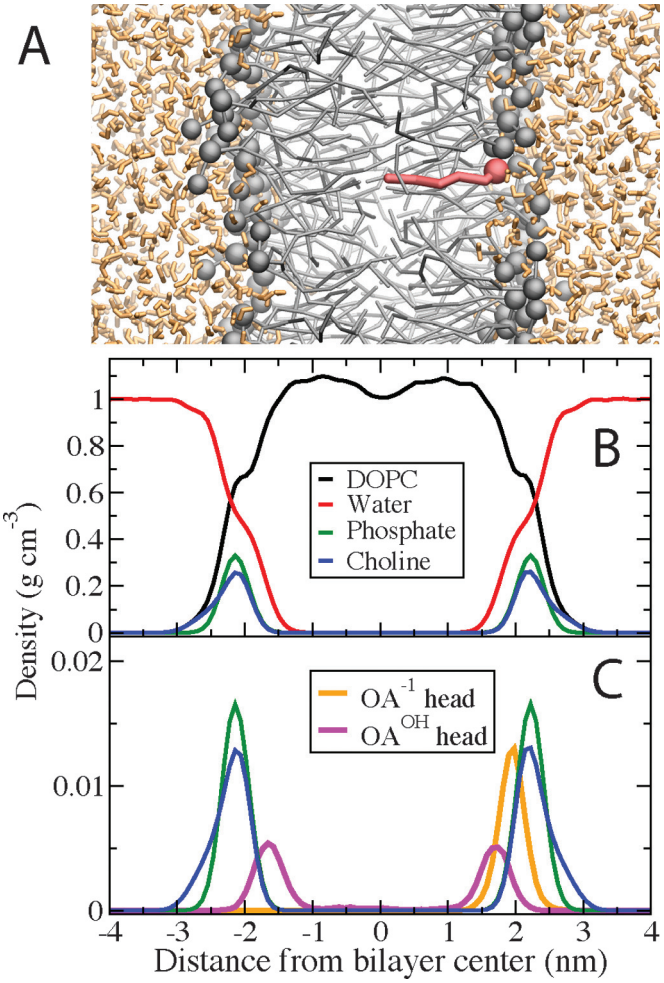

interesting to try the new parameters we recently developed for aspartate for the MARTINI 2.2 amino acid force field[37] with constant pH MD simulations. These parameters were shown to better reproduce the side chain partitioning in a DOPC bilayer than MARTINI 2.1.

The broad distribution of individual monomers for the 20- and 30-mer in Fig. 4 (grey and brown symbols) illustrates incomplete sampling. Because each OA is an independent sample, over a long enough timescale the time averaged mean protonation state for each monomer should be equal to the mean for the aggregate. This is a stark reminder of the sampling required for surfactant systems, where 100 ns is insufficient for a small 20-mer.

Future directions

We show this is as a promising new method for studying coarse-grained systems of aggregating amphiphiles, and likely for many protein and lipid bilayer systems. Further testing and refinement may be needed, such as the effect of counter charges, salt concentration, box size, and long-range electrostatics. There are many interesting avenues for future research given the importance of pH and the ability to model aggregation of small molecules.

Conclusions

We have combined MARTINI coarse-grained simulations and constant pH MD to study the titration behavior of small aggregates of oleic acid and oleic acid in a DOPC bilayer. The titration behavior of oleic acid is shown to depend on the local chemical environment. In small micelles, the pK_a of oleic acid increases and we observe a large degree of anticooperativity. The agreement between experiment and CG simulations for the pK_a of oleic acid in PC bilayers is a good validation for the model. We anticipate future work into this combination of CG models with constant pH simulations.

Acknowledgements

This work is supported by the Natural Sciences and Engineering Research Council of Canada (NSERC). WFDB is supported by Alberta Innovates Health Solutions (AIHS) studentships. DPT is an AIHS Scientist and Alberta Innovates Technology Futures Strategic Chair in (Bio)Molecular Simulation. Simulations were carried out on WestGrid/Compute Canada facilities. GG is supported by the Academy of Finland. We thank Dr. Helmut Grubmüller for feedback on an earlier draft of the manuscript.

References

(1) Markvoort, A. J.; Pfleger, N.; Staffhorst, R.; Hilbers, P. A. J.; Van Santen, R. A.; Killian, J. A.; De Kruijff, B. *Biophys. J.* **2010**, *99*, 1520. doi:10.1016/j.bpj.2010.06.057.
(2) Chen, I. A.; Szostak, J. W. *Proc. Natl. Acad. Sci. U.S.A.* **2004**, *101*, 7965. doi:10.1073/pnas.0308045101.
(3) Fedorenko, A.; Lishko, P. V.; Kirichok, Y. *Cell* **2012**, *151*, 400. doi:10.1016/j.cell.2012.09.010.
(4) Severin, F. F.; Severina, I. I.; Antonenko, Y. N.; Rokitskaya, T. I.; Cherepanov, D. A.; Mokhova, E. N.; Vyssokikh, M. Y.; Pustovidko, A. V.; Markova, O. V.; Yaguzhinsky, L. S.; Korshunova, G. A.; Sumbatyan, N. V.; Skulachev, M. V.; Skulachev, V. P. *Proc. Natl. Acad. Sci. U.S.A.* **2010**, *107*, 663. doi:10.1073/pnas.0910216107.
(5) Ponnurangam, S.; Chernyshova, I. V.; Somasundaran, P. *Langmuir* **2012**, *28*, 10661. doi:10.1021/la300995g.
(6) Fischer, C. L.; Drake, D. R.; Dawson, D. V.; Blanchette, D. R.; Brogden, K. A.; Wertz, P. W. *Antimicrob. Agents Chemother.* **2012**, *56*, 1157. doi:10.1128/AAC.05151-11.
(7) Cistola, D. P.; Hamilton, J. A.; Jackson, D.; Small, D. M. *Biochemistry* **1988**, *27*, 1881. doi:10.1021/bi00406a013.
(8) Cistola, D. P.; Atkinson, D.; Hamilton, J. A.; Small, D. M. *Biochemistry* **1986**, *25*, 2804. doi:10.1021/bi00358a011.
(9) Budavari, S. Inc., Whitehouse Station, NJ, 1996.
(10) Notman, R.; Noro, M. G.; Anwar, J. *J. Phys. Chem. B* **2007**, *111*, 12748. doi:10.1021/jp0723564.
(11) Turner, D. C.; Yin, F.; Kindt, J. T.; Zhang, H. *Langmuir* **2010**, *26*, 4687.
(12) King, D. T.; Warren, D. B.; Pouton, C. W.; Chalmers, D. K. *Langmuir* **2011**, *27*, 11381. doi:10.1021/la2022903.
(13) Ngo, V. A.; Kalia, R. K.; Nakano, A.; Vashishta, P. *J. Phys. Chem. B* **2012**.
(14) Cerezo, J.; Zuniga, J.; Bastida, A.; Requena, A.; Ceron-Carrasco, J. P. *J. Phys. Chem. B* **2011**, *115*, 11727. doi:10.1021/jp203498x.
(15) Morrow, B. H.; Wang, Y.; Wallace, J. A.; Koenig, P. H.; Shen, J. K. *J. Phys. Chem. B* **2011**, *115*, 14980. doi:10.1021/jp2062404.
(16) Morrow, B. H.; Koenig, P. H.; Shen, J. K. *J. Chem. Phys.* **2012**, *137*, 194902. doi:10.1063/1.4766313.
(17) Mongan, J.; Case, D. A.; McCammon, J. A. *J. Comput. Chem.* **2004**, *25*, 2038. doi:10.1002/jcc.20139.
(18) Lee, M. S.; Salsbury, F. R.; Brooks, C. L. *Proteins: Struct., Funct., Bioinform.* **2004**, *56*, 738. doi:10.1002/prot.20128.
(19) Khandogin, J.; Brooks, C. L., III. *Biophys. J.* **2005**, *89*, 141. doi:10.1529/biophysj.105.061341.
(20) Donnini, S.; Tegeler, F.; Groenhof, G.; Grubmüller, H. *J. Chem. Theory Comput.* **2011**, *7*, 1962. doi:10.1021/ct200061r.
(21) Borjesson, U.; Hünenberger, P. H. *J. Chem. Phys.* **2001**, *114*, 9706. doi:10.1063/1.1370959.
(22) Shih, A. Y.; Arkhipov, A.; Freddolino, P. L.; Schulten, K. *J. Phys. Chem. B* **2006**, *110*, 3674. doi:10.1021/jp0550816.
(23) Kasson, P. M.; Kelley, N. W.; Singhal, N.; Vrljic, M.; Brunger, A. T.; Pande, V. S. *Proc. Natl. Acad. Sci. U.S.A.* **2006**, *103*, 11916. doi:10.1073/pnas.0601597103.
(24) Marrink, S. J.; de Vries, A. H.; Tieleman, D. P. *Biochim. Biophys. Acta Biomem.* **2009**, *1788*, 149. doi:10.1016/j.bbamem.2008.10.006.
(25) Baoukina, S.; Marrink, S. J.; Tieleman, D. P. *Biophys. J.* **2012**, *102*, 1866. doi:10.1016/j.bpj.2012.03.048.
(26) Shinoda, W.; Devane, R.; Klein, M. *Molecular Simulation* **2007**, *33*, 27. doi:10.1080/08927020601054050.

(27) Marrink, S. J.; Risselada, H. J.; Yefimov, S.; Tieleman, D. P.; de Vries, A. H. *J. Phys. Chem. B* **2007**, *111*, 7812. doi:10.1021/jp071097f.
(28) Yesylevskyy, S. O.; Schäfer, L. V.; Sengupta, D.; Marrink, S. J. *PLoS Comput. Biol.* **2010**, *6*, e1000810. doi:10.1371/journal.pcbi.1000810.
(29) Berendsen, H. J. C.; Postma, J. P. M.; Van Gunsteren, W. F.; Dinola, A.; Haak, J. R. *J. Chem. Phys.* **1984**, *81*, 3684. doi:10.1063/1.448118.
(30) Van der Spoel, D.; Lindahl, E.; Hess, B.; Groenhof, G.; Mark, A. E.; Berendsen, H. J. *J. Comput. Chem.* **2005**, *26*, 1701. doi:10.1002/jcc.20291.
(31) Berendsen, H. J. C.; Van der Spoel, D.; Van Drunen, R. *Comput. Phys. Commun.* **1995**, *91*, 43. doi:10.1016/0010-4655(95)00042-E.
(32) Kirkwood, J. G. *J. Chem. Phys.* **1935**, *3*, 300.
(33) MacCallum, J. L.; Bennett, W.; Tieleman, D. P. *Biophys. J.* **2008**, *94*, 3393. doi:10.1529/biophysj.107.112805.
(34) Ptak, M.; Egret-Charlier, M.; Sanson, A.; Bouloussa, O. *Biochim. Biophys. Acta Biomem.* **1980**, *600*, 387. doi:10.1016/0005-2736(80)90442-3.
(35) Small, D. M.; Cabral, D. J.; Cistola, D. P.; Parks, J. S.; Hamilton, J. A. *Hepatology* **1984**, *4*, 77S. doi:10.1002/hep.1840040814.
(36) Bennett, W. F. D.; Tieleman, D. P. *J. Chem. Theory Comput.* **2011**, *7*, 2981. doi:10.1021/ct200291v.
(37) de Jong, D. H.; Singh, G.; Bennett, W. F. D.; Arnarez, C.; Wassenaar, T. A.; Schäfer, L. V.; Periole, X.; Tieleman, D. P.; Marrink, S. J. *J. Chem. Theory Comput.* **2012**, *9*, 687. doi:10.1021/ct300646g.